Korean J. Chem. Eng., 36(7), 1021-1032 (2019)
DOI: 10.1007/s11814-019-0247-5

pISSN: 0256-1115
eISSN: 1975-7220

Stratified electromagnetohydrodynamic flow of nanofluid supporting convective role

Yahaya Shagaiya Daniel[*,,***], Zainal Abdul Aziz[*,**,†], Zuhaila Ismail[*,**], Arifah Bahar[*,**], and Faisal Salah[****]**

*Department of Mathematical Sciences, Faculty of Science, Universiti Teknologi Malaysia, 81310 UTM Johor Bahru, Johor, Malaysia
**UTM Centre for Industrial and Applied Mathematics (UTM-CIAM), Ibnu Sina Institute for Scientific and Industrial Research (ISI-SIR) Universiti Teknologi Malaysia, 81310 UTM Johor Bahru, Johor, Malaysia
***Department of Mathematical Sciences, Faculty of Science, Kaduna State University, Tafawa Belewa Way, P.M.B 2339. Kaduna State, Nigeria
****Department of Mathematics, College of Science & Art, King Abdul-Aziz University, 21589, Saudi Arabia
(*Received 30 October 2018 • accepted 21 February 2019*)

Abstract−This study numerically examined unsteady double stratified EMHD mixed convection flow of nanofluid via permeable stretching sheet. It also looked at the convective heat and mass boundary conditions as well as the Navier velocity slip. In the thermal field, the effects of radiative heat transfer, heat generation/absorption, viscous dissipation, together with Ohmic heating (both magnetic and electric fields) were considered. The concentration field accounts for the chemical reaction. These show the physical behavior of electromagnetohydrodynamic flow associated with the problem formulation. The characteristics in regard to convective heat and mass, Navier slips conditions, as well as double stratification, were imposed. Such structure arises in energy efficiency and performance, which is achievable without higher pumping power, serves in the extrusion manufacturing process involving the thermal system for efficient devices particularly in polymeric, paper production, and food processing. The governing equations, which are nonlinear partial differential equations, were modelled by ordinary differential equations using suitable transformations. The ODEs were solved numerically, using implicit finite difference method (Keller box method). The physical implications deliberated on the behavior via the velocity, thermal energy, and concentration fields as well as the skin friction coefficient; the Nusselt and Sherwood numbers were scrutinized in relation to several parameters via mathematical model. The analysis shows that thermal and concentration stratifications decrease the distributions adjacent to the sheet surface, indicating decrease in the concentration nanoparticles and reduction in thermal energy. Augmentation occurs with convective heat and mass Biot numbers with the fields. The electric and magnetic parameters exhibit opposite flow behavior to the velocity and temperature. Chemical reaction and viscous dissipation weaken the concentration profile. Numerical results were compared with the published data available in the literature for limiting cases, and good agreement was noticed.

Keywords: EMHD Nanofluid, Thermal Radiation, Chemical Reaction, Stratification, Convective Conditions

INTRODUCTION

The study of mixed convection flow of nanofluids with chemical reaction over a stretching surface has vital roles in chemical and metallurgy engineering industries. In essence, heat convection occurs in wet cooling towers, during drying processes, moisture over agricultural fields, processing of food, temperature/concentration transfer, destruction of crops in freezing condition, polymer production, motion in a desert cooler, evaporation over the surface (water body), and others [1,2].

Study on heat and mass transfer, along with chemical reactions, has significant value in various industries and has gained the attention of researchers recently. Chemical reaction occurs between two or more chemicals, which leads to the transformation of substances [3-5]. Conventional heat transfer occurring in oil, water, and ethylene glycol mixtures are poor heat transfer fluids due to the low thermal conductivity.

Nanofluids have the potential to reduce thermal resistance in many applications, such as cooling in electronics chips, drug delivery, food processing, and emission reduction. Such fluids usually contain a suspension of nanosized (10^{-9}-10^{-7} m) particles from metals or nonmetallic materials into base fluids [6]. The impact of gold nanoparticles on MHD mixed convection Poiseuille flow induced by external pressure gradient and buoyancy force was studied [7]. Results signified that metals have a higher rate of heat transfer than metal oxides. Xiao et al. [8] explored the facile one-pot aqueous-phase synthesis of PdAu bimetallic nanoparticles with different Pd/Au ratios. The presence of nanoparticles is to enrich the heat transfer performance of the ordinary heat transfer liquids. The high cooling rate expectation becomes impossible with the conventional fluid, due to poor thermal conductivity. Brownian motion and thermophoretic force features traced on the nanoparticles extensively contributes towards enhancing the thermal conductivity of based fluids [9,10].

†To whom correspondence should be addressed.
E-mail: zainalaz@utm.my

In view of the above analysis, the study conducted numerical analysis on unsteady MHD flow of cross nanofluid over a stretching surface with non-linear radiation influence [11]. The Buongiorno nanofluid model was implemented to scrutinize the effects of thermophoresis and Brownian motion. Impact of activation energy over the chemically reactive radiative flow of Carreau nanofluid due to nonlinearly mixed convection was considered by Irfan et al. [12]. Based on their findings, higher values of the magnetic field, Brownian motion, and thermophoretic parameters tend to increase the thermal energy of the Carreau nanofluid. Sheikholeslami [13] studied the shape factor and Brownian motion impact on nanofluid modeling. Results prove that convection decreases with increase in magnetic forces. The magnetic nanoparticles are also useful in manufacturing magnetic cell separation, loudspeakers, drug delivery, magnetic resonance imaging, cancer treatment with magnetic hyperthermia, etc. [14,15]. Khan et al. [16] examined partial slip characteristics and entropy generation in MHD mixed convection flow by the stretchable rotating disk. Interestingly, the velocity gradient decreases via a magnetic field, slip variable, and suction parameter.

Many investigations of MHD mixed convection heat and mass transfer against vertical stretching sheet were done in recent years due to their applications in the area of engineering such as cooling of electronic components, thermal insulation, solar collectors, as well as designing buildings [17-20]. The impact of thermal radiation is crucial to space technology and high-temperature processes. Influence of nonlinear radiation using ferrofluid flow was deliberated by Rashid et al. [21]. Their work incorporated viscous dissipation and Joule heating. Temperature is enhanced for the radiation parameter, Eckert number, and heat generation parameter. Thermal radiation helps in controlling heat convection process in polymer processing. Reduction in thermal resistance of heat transfer within the fluids would undoubtedly enhance diverse applications/processes.

Stratification flow has gained attention due to its significant expediency in heat and mass transfer beside natural procedures. The influence of gyrotactic microorganisms for the 2D stratified flow of an Oldroyd-B nanomaterial was highlighted by Waqas et al. [22]. Applied magnetic field along with mixed convection was considered in the mathematical formulation. The analysis of double stratification in MHD flow of nanofluid by a stretching cylinder was carried out by Hayat et al. [23]. Brownian motion and thermophoresis impacts are presented in the transport equations. They studied a fluid having density fluctuations in the vertical bearing (perpendicular direction) in relation to a stratified fluid. Concentration as well as temperature variations or dissolved phases with varies densities account for the stratification generation. Inherently, some applications of stratification are on convection of heat from thermal sources in power plant condensers, heat rejection from lake surroundings, thermal storage system in solar ponds, geothermal systems, heterogeneous mixtures in the atmosphere, etc [24-26]. Simultaneous rise in both mass and heat transfer leads to double stratification [27]. These significantly play an important role in regulating the concentration as well as the temperature variations of oxygen and hydrogen in water bodies (ponds and lakes), which greatly affects growth in species. It is significant to examine double stratification impacts on heat and mass transfer arise concurrently. These keep balance levels of hydrogen and oxygen for excellent growth progression in species for enrichment beside energy efficiency in devices [28-30].

Convective heat and mass transport at the surface are ordered as the main class of convective fluid temperature/concentration. Heat and mass transfer convective fluid over surface define a convective heat exchange condition for entities in thermal and concentration fields, quantified heat capacity [31]. The heat and mass transfer with convective boundary conditions cause considerable change in processes, essentially inducing high temperatures. These are found in systems of thermal energy storage, petroleum industry, gas turbines, nuclear plants, conjugate heat transport, heat exchangers, etc. [32]. In view of the above analysis, convective mass condition was introduced on the 2D MHD boundary layer flow of nanofluid. Shehzad et al. [33] discussed the case with the existence of an applied magnetic field. Heat and mass transfer characteristics were explored by convective boundary conditions on hydromagnetic stagnation point flow of thixotropic nanofluid towards over a stretching surface by Hayat et al. [34]. The convective boundary conditions cause temperature slip relative to the convective fluid temperature at the wall, which is suddenly affected by the mass transfer. The temperature fluid is quite different from the prescribed wall temperature. Better quality product from industry can be achieved through good application based on heat and mass transfer processes.

The main aim of this study was to explore double stratification through convective heat and mass conditions on unsteady MHD mixed convection slip flow of nanofluid over a stretching sheet with the electric field effects. It considers the physical characteristics of electromagnetohydrodynamic flow with respect to stretching sheet. In addition to the thermal field are thermal radiation, viscous dissipation and Ohmic heating (electric and magnetic fields) in the presence of heat generation/absorption. The concentration field has an impact on the chemical reaction. The motion is electrically conducted via a couple of electric and magnetic fields. Heat including mass transport was engaged further down with the Brownian movement beside thermophoretic force. Convective heat and mass situations were considered over the model. Numerical simulation, Keller box scheme, was used to tackle the governing scientific flow model. A number of characteristics involving physical constraints on the flow distribution, thermal energy distribution, nanoparticle-concentration distribution, skin friction coefficient distribution, the Nusselt number and Sherwood numbers were visualized via plots and numerical data. Current results were compared with the available published data in the restrictive case and good agreement was obtained.

FORMULATION

1. Flow Scrutiny

Consider an unsteady two-dimensional mixed convection transport of an incompressible electrically-conducting nano-liquid over a linear permeable stretching sheet (see Fig. 1) with velocity designated as $u_w(x)=bx/(1-at)$, where b represents stretching rate as a denotes constant obligating $(\text{time})^{-1}$ dimensionless for ($at<1$, $\alpha\geq 0$). Magnetic field denoted by $B=B_0/\sqrt{1-at}$, along with an electric field $E=E_0/\sqrt{1-at}$ is applied normal to the flow field [35]. In this situa-

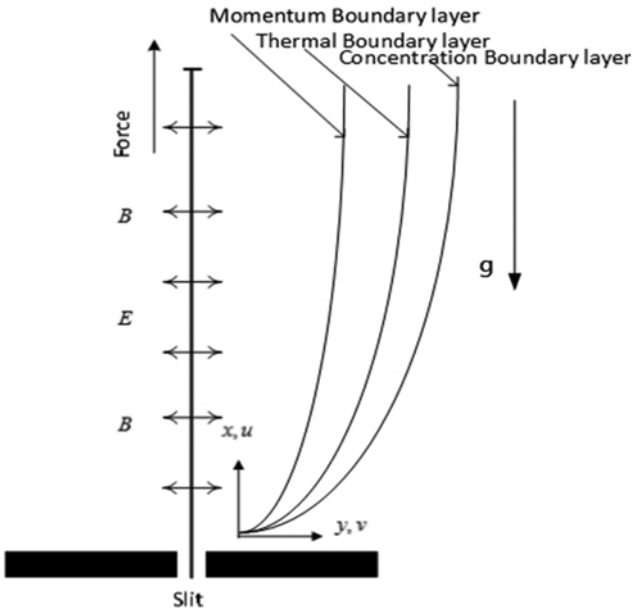

Fig. 1. Physical flow geometry.

tion the magnetic-Reynolds variable is negligible. Also, induced-magnetic-field is insignificant in contrast to the applied-magnetic-field. Therefore, the induced magnetic field is inconsequential as well as the magnetic-Reynolds-constant. The variable T denotes the temperature, φ the concentration, and g is gravitational acceleration respectively. The equations governing the flow are presented as:

$$\frac{\partial u}{\partial x}+\frac{\partial v}{\partial y}=0 \tag{1}$$

$$\frac{\partial u}{\partial t}+u\frac{\partial u}{\partial x}+v\frac{\partial u}{\partial y}=\upsilon\left(\frac{\partial^2 u}{\partial y^2}\right)+\frac{\sigma}{\rho_f}(EB-B^2u)+\frac{1}{\rho_f}[(1-\varphi_\infty)\rho_{f\infty}\beta_T(T-T_\infty)-(\rho_p-\rho_{f\infty})\beta_\varphi(\varphi-\varphi_\infty)]g \tag{2}$$

with the boundary conditions [36]:

$$y=0:\ u=u_w+l_1\frac{\partial u}{\partial y},\ v=v_w, \tag{3}$$

$$y\to\infty:\ u\to 0. \tag{4}$$

Here (u, v) represents velocity components in the x- and y-directions, respectively; $v_w=-v_0/\sqrt{1-at}$ symbolizes wall mass transfer (taken injection as ($v_w<0$), whereas suction depicts ($v_w>0$)), $l_1=l_1'\sqrt{1-at}$, σ, β_T, ρ_f, and β_φ represents slip velocity factor, electrical conductivity, coefficient of thermal expansion, fluid density, and the mass diffusion coefficient, respectively.

Using the following transformations,

$$\psi=\sqrt{\frac{b\upsilon}{1-at}}xf(\eta),\ \eta=y\sqrt{\frac{b}{\upsilon(1-at)}},\ \theta=\frac{T-T_\infty}{T_f-T_0},\ \phi=\frac{\varphi-\varphi_\infty}{\varphi_f-\varphi_0}, \tag{5}$$

with the stream function ψ defined as:

$$u=\frac{\partial\psi}{\partial y},\ v=-\frac{\partial\psi}{\partial x} \tag{6}$$

Continuity Eq. (1) is satisfied and Eq. (2) is reduced as follows:

$$f'''+ff''-f^2-\delta\left(f'+\frac{\eta}{2}f''\right)+M(E_1-f')+\lambda(\theta-N\phi)=0, \tag{7}$$

with the boundary conditions

$$f=s,\ f'=1+Lf'',\ \text{at}\ \eta=0;\ f'=0,\ \text{as}\ \eta\to\infty. \tag{8}$$

where f′, θ, and ϕ are the dimensionalized variables representing the velocity, temperature, and nanoparticles concentration, respectively; s is the suction/injection parameter, δ=a/b stands for the unsteadiness parameter, λ=Gr/Re^2 is the mixed convection parameter, $Gr=g\beta(1-\varphi_\infty)(T_f-T_0)x^3/\upsilon^2$ is the Grashof number (T_0 is the reference temperature, and $T_f=T_0+A_1x/(1-at)$ represents the heated fluid temperature (where A_1 is dimensional constant)), $\varphi_f=\varphi_0+C_1x/(1-at)$ represents the heated fluid concentration (C_1 is dimensional constant), $N=(\rho_p-\rho_{f\infty})(\varphi_f-\varphi_0)/\beta(1-\varphi_\infty)(T_f-T_0)$ denotes the buoyancy ratio parameter, $Re=u_wx/\upsilon$ is the Reynolds number, $L=l_1'\sqrt{b/\upsilon}$ is the parameter slip velocity, and $E_1=E_0/u_wB_0$ is the parameter electric field and $M=\sigma B_0^2/b\rho_f$ is the parameter magnetic field.

Skin friction coefficient can be defined as follows:

$$c_f=\frac{\tau_w}{\rho u_x^2(x,t)}, \tag{9}$$

where

$$\tau_w=\mu\left(\frac{\partial u}{\partial y}\right)_{y=0}, \tag{10}$$

In this direction, τ_w takes the shear stress along the stretching sheet involving the nanofluid. The coefficient of the local skin-friction in non-dimensional form follows:

$$Re^{1/2}c_f=f''(0), \tag{11}$$

2. Energy Equation

Energy equation deals with the thermal radiation, viscous dissipation as a consequence of the Ohmic heating with a convectively heating stretching sheet. The impact of heat generation or absorption besides the thermal stratification were considered, in view, of the Rosseland approximation of radiation [37,38]:

$$\frac{\partial T}{\partial t}+u\frac{\partial T}{\partial x}+v\frac{\partial T}{\partial y}=\frac{k}{(\rho c)_f}\left(\frac{\partial^2 T}{\partial y^2}\right)+\frac{1}{(\rho c)_f}\left(\frac{16T_\infty^3\sigma^*}{3k^*}\frac{\partial^2 T}{\partial y^2}\right)+\frac{\mu}{(\rho c)_f}\left(\frac{\partial u}{\partial y}\right)^2+\frac{Q}{(\rho c)_f}(T-T_\infty)+\tau\left\{D_B\left(\frac{\partial\varphi}{\partial y}\frac{\partial T}{\partial y}\right)+\frac{D_T}{T_\infty}\left(\frac{\partial T}{\partial y}\right)^2\right\}+\frac{\sigma}{(\rho c)_f}(uB-E)^2. \tag{12}$$

with condition at the boundary [39]:

$$y=0:\ -k\frac{\partial T}{\partial y}=h_f(T_f-T), \tag{13}$$

$$y\to\infty:\ T\to T_\infty=T_0+\frac{A_2x}{1-at}. \tag{14}$$

where σ^* is the mean absorption coefficient, and k^* characterizes Stefan-Boltzmann variable. The other constants h_f, $\alpha=k/(\rho c)_f$, μ, ρ, c_p are the convective heat transfer coefficient, the thermal-diffusivity connected the fluid, fluid kinematic-viscosity, the fluid density and specific heat respectively. Also, $Q=Q_0/(1-at)$ represents the

non-uniform heat generation/absorption coefficient (Q_0 is powerful uniform heat generation or the absorption variable), k denotes the thermal conductivity, A_2 is the dimensional constant, D_B is the coefficient of Brownian diffusion, D_T represents the coefficient of thermophoresis diffusion, $\tau=(\rho c)_p/(\rho c)_f$ is the heat transfer capacity with respect to the nanoparticle divided by the heat capacity with respect to the liquid.

Bringing together the defined variables in Eq. (5) along with Eqs. (12)-(14), results in:

$$\frac{1}{\mathrm{Pr}}\left(1+\frac{4}{3}\mathrm{Rd}\right)\theta''+\mathrm{f}\theta'-\mathrm{f}'\theta-\mathrm{s}_t\mathrm{f}'-\delta\left(\mathrm{s}_t+\frac{\eta}{2}\theta'+2\theta\right)+\mathrm{Nb}\phi'\theta' \quad (15)$$

$$+\mathrm{Nt}\theta^2+\mathrm{Ec}(\mathrm{f}'')^2+\varepsilon\theta+\mathrm{MEc}(\mathrm{f}'-\mathrm{E}_1)^2=0.$$

With defined boundary conditions,

$$\theta'=-\mathrm{B}_{i1}(1-\mathrm{s}_t-\theta),\ \text{at}\ \eta=0;\ \theta=0,\ \text{as}\ \eta\to\infty. \quad (16)$$

Here, $\mathrm{B}_{i1}=(\mathrm{h}_f/\mathrm{k})\sqrt{\upsilon/\mathrm{b}}$ denotes the thermal Biot number, $\mathrm{Nb}=(\rho c)_p D_B(\varphi_f-\varphi_0)/(\rho c)_f\upsilon$ represents Brownian motion constant, $\mathrm{Nt}=(\rho c)_p D_T(T_f-T_0)/(\rho c)_f\upsilon T_\infty$ is the thermophoresis constant, $\mathrm{Ec}=u_w^2/c_p(T_f-T_0)$ is the Eckert number, $\mathrm{Pr}=\upsilon/\alpha$ is the Prandtl number, $s=v_0/\sqrt{\upsilon b}$ the suction parameter, $\mathrm{Rd}=4\sigma^*T_\infty^3/k^*k$ the thermal radiation parameter, $s_t=A_2/A_1$ the thermal stratification parameter, and $\varepsilon=Q_0/b(\rho c)_f$ denotes heat generation ($\varepsilon>0$) or absorption ($\varepsilon<0$) also when $\varepsilon=0$ indicates absence of heat generation/absorption effects.

The Nusselt number is defined as follows:

$$\mathrm{Nu}=\frac{\mathrm{x}q_w}{\mathrm{k}(T_f-T_0)}, \quad (17)$$

where q_w represents the surface heat flux, expressed as:

$$q_w=-\left(\left(\mathrm{k}+\frac{16\sigma^*T_\infty^3}{3k^*}\right)\frac{\partial T}{\partial y}\right)_{y=0}, \quad (18)$$

The Nusselt number in non-dimensional-form can be defined as:

$$\mathrm{Nu}/\mathrm{Re}^{1/2}=-\left(1+\frac{4}{3}\mathrm{Rd}\right)\left(\frac{1}{1-s_t}\right)\theta'(0), \quad (19)$$

3. Mass Transfer

Convective mass flow impact over nanoparticle concentration as regards to concentration stratification and the homogeneous-chemical-reaction for first order is modelled as:

$$\frac{\partial\varphi}{\partial t}+u\frac{\partial\varphi}{\partial x}+v\frac{\partial\varphi}{\partial y}=D_B\left(\frac{\partial^2\varphi}{\partial y^2}\right)+\frac{D_T}{T_\infty}\left(\frac{\partial^2 T}{\partial y^2}\right)-k_1(\varphi-\varphi_\infty). \quad (20)$$

with boundary conditions:

$$y=0:\ -D_B\frac{\partial\varphi}{\partial y}=h_g(\varphi_f-\varphi) \quad (21)$$

$$y\to\infty:\ \varphi\to\varphi_\infty=\varphi_0+\frac{C_2x}{1-at} \quad (22)$$

Such that φ_f, φ_0, $k_1=k_0/(1-at)$, h_g, D_B, C_2 and $\varphi_f=\varphi_0+C_1x/(1-at)$ denote the variable concentration of the hot fluid, the concentration at the surface, the rate of chemical reaction, the variable mass transfer coefficient, Brownian diffusion coefficient, dimension constant and the heated fluid concentration (i.e. C_1 is dimensional constant), respectively.

Employing the transforms in Eq. (5) into Eqs. (20)-(22), we get

$$\phi''+\mathrm{Scf}\phi'-\mathrm{Scf}'\phi-\mathrm{Scs}_m\mathrm{f}'-\delta\mathrm{Sc}\left(\mathrm{s}_m+\frac{\eta}{2}\phi'+\phi\right)+\frac{\mathrm{Nt}}{\mathrm{Nb}}\theta''-\mathrm{Sc}\gamma\phi=0 \quad (23)$$

Subjected to boundary condition:

$$\phi'=-\mathrm{B}_{i2}(1-\mathrm{s}_m-\phi),\ \text{at}\ \eta=0;\ \phi=0,\ \text{as}\ \eta\to\infty \quad (24)$$

Here, $\mathrm{B}_{i2}=(h_g/D_B)\sqrt{\upsilon/b}$ is the mass Biot number, $s_m=C_2/C_1$ is the mass stratification parameter, $\gamma=k_0/b$ denotes the chemical reaction constant ($\gamma>0$ takes the destructive chemical reaction parameter, and $\gamma<0$ is generative chemical reaction parameter) [40].

The Sherwood number is defined as follows:

$$\mathrm{Sh}=\frac{\mathrm{x}q_m}{D_B(\varphi_f-\varphi_0)}, \quad (25)$$

where

$$q_m=-D_B\frac{\partial\varphi}{\partial y}_{y=0}, \quad (26)$$

q_m is surface-mass-flux of the nanofluid.

The Sherwood number is presented in a non-dimensional form as:

$$\mathrm{Sh}/\mathrm{Re}^{1/2}=-\left(\frac{1}{1-s_m}\right)\phi'(0), \quad (27)$$

ANALYSIS

The ordinary differential equations which are highly nonlinear (7), (15), and (23) subjected to the boundary conditions (8), (16), are (24) are solved numerically (Keller box scheme [41]). The physical significance of the dimensionless parameters and their range of variation are presented [35,42-47] for selection of values in the parametric study. As justification of the current numerical method, the outcomes were obtained and scrutinized with published works of [43,45] and [48] in a few restrictive situations when. The accessible computational values are in good agreement as compared to others, as shown in Table 1, for the coefficient of the skin friction generated.

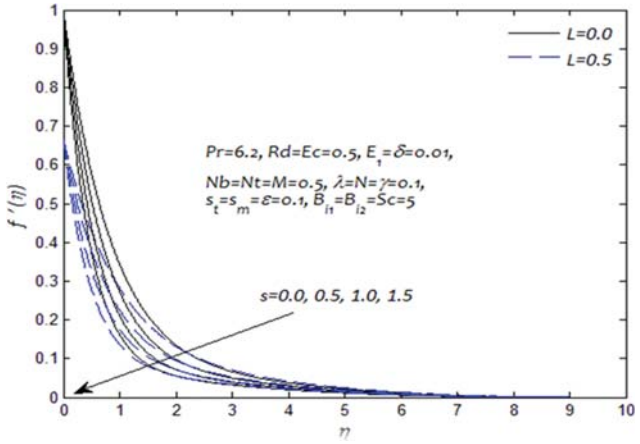

Fig. 2. Strength of s on the velocity distribution $f'(\eta)$.

Table 1. Comparison over coefficient of the skin friction $-f''(0)$ when $E_1=\lambda=L=N=0$

M	s	δ	Khan and Azam [48]	Ibrahim and Shankar [43]	Hayat et al. [45]	Present results
0.0	0.0	0.0	-	1.0000	-	1.000000
	0.5		-	1.2808	1.2808	1.280776
0.5	0.5		-	1.5000	-	1.500000
1.0	0.5		-	1.6861	-	1.686141
	0.0			1.4142		1.414214
	0.2			1.5177		1.517745
	0.7			1.8069		1.806880
	1.0			2.000		2.000000
1.5	0.5		-	1.8508	-	1.850781
2.5	0.5		-	2.0000	-	2.000000
1.0	0.0		-	1.4142	1.4142	1.414214
5.0			-	-	2.4494	2.449490
0.0		0.0	1.0000	-	-	1.000000
		0.2	1.06801	-	-	1.068012
		0.4	1.13469	-	-	1.134685
		0.6	1.19912	-	-	1.199117
		0.8	1.26104	-	-	1.261040
		1.2	1.37772	-	-	1.377720
		1.4	1.43284	-	-	1.432831
		2.0	1.58737	-	-	1.587358

1. Velocity Profiles

Fig. 2 demonstrates the behavior of suction s and velocity slip L on the velocity profile. The nanofluid motion gradually decreases under the strengths of slip conditions (L>0), for a rise in suction (s>0), as the velocity profile drops. The outcomes strongly depend on the power law existing between the slip flow and the shear stress at the wall, due to non-adherence of the fluid to a solid boundary. At impermeable (s=0.0) and no-slip (L=0.0) stages, the flow is at maximum level up-direction the vertical direction on the surface. A higher magnitude of suction parameter gives way to resistance to the fluid flow resulting in decrease in the velocity. Note that the velocity profile increases at the surface of the stretching sheet for a small amplitude of the suction parameter. Both parameters reduce the velocity distribution for higher values.

In Fig. 3 exhibits the behavior of mixed convection parameter λ and electric field parameter E_1 on the velocity profile. The nanofluid flow along the stretching sheet is minimal at force convection flow locale (λ=0.0) alongside with absence of an electric field (E_1=0.0). For heated stretching surface locale (λ>0), the convection current augments the nanofluid flow greatly subject to the electric field ($E_1\neq$0.0). Applying the electric field intensified natural convective heat transfer of nanofluid. The natural convection current is controlled by the forced convection of the fluid molecules and nanoparticles along the stretching sheet flow direction. Augmentation of the mixed convection parameter and electric field enhances the buoyancy force, which boosts the velocity and the

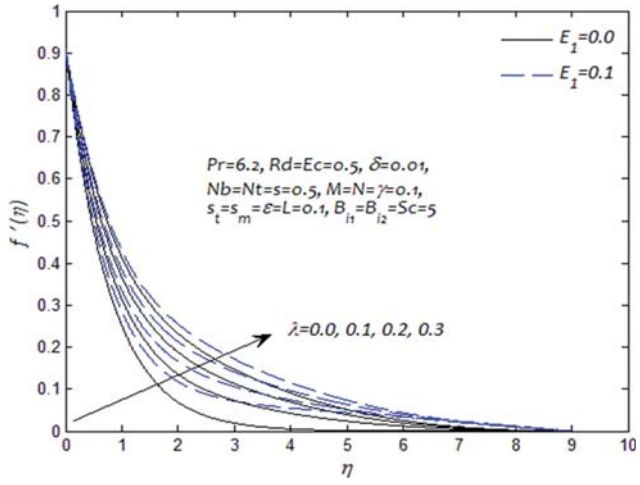

Fig. 3. Strength of λ on the velocity distribution $f'(\eta)$.

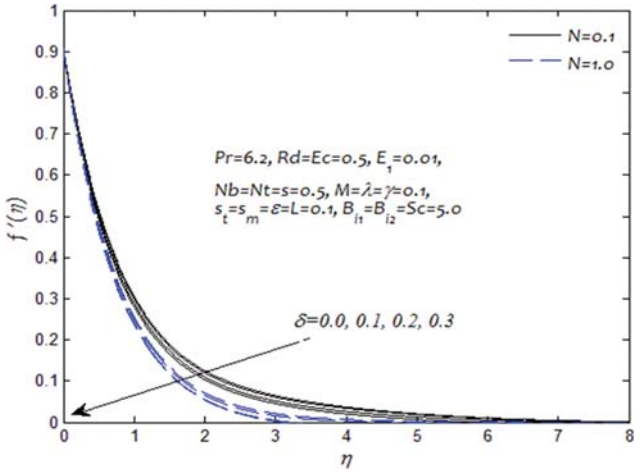

Fig. 4. Strength of δ on the velocity distribution $f'(\eta)$.

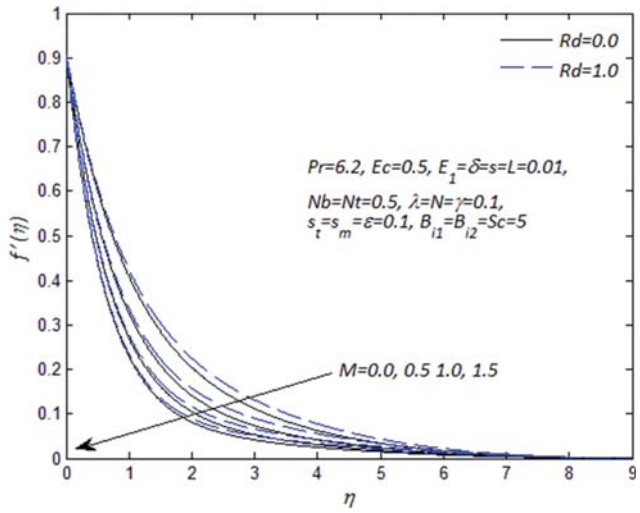

Fig. 5. Strength of M on the velocity distribution f′(η).

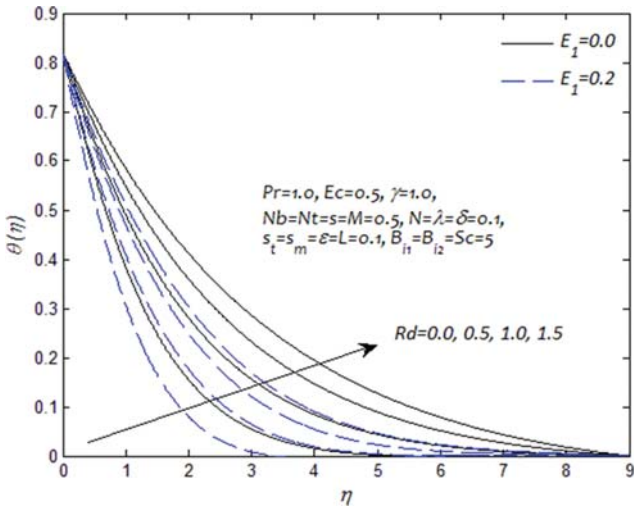

Fig. 6. Strength of Rd on the temperature distribution θ(η).

momentum boundary layer thickness. Electric field creates room for the fluid molecules-particles intensifications in such a way that the Lorentz force tends to strengthen the physical forces which resulted in boosting the flow of the nanofluid velocity.

The consequence connected with unsteadiness parameter δ with respect to the acceleration case (δ>0) and the ratio of concentration to thermal buoyancy forces over the fluid velocity are represented in Fig. 4. The velocity profile decreased for the higher acceleration case (δ>0), lower with an effect of the buoyancy ratio parameter. This results in a thinner momentum boundary-layer. The nanofluid flow behavior decreases across the vertical surface due to prevailing strengths from the stretching sheet constant. This causes the momentum boundary-layer thickness to be lower for a high amplitude of the buoyancy ratio and unsteadiness parameters.

Fig. 5 depicts the impacts of magnetic and thermal radiation on the velocity profile. The velocity profile is reduced with the rising of the magnetic field, conversely with thermal radiation. The Lorentz force related to the magnetic field rises, leading to significant resistance to the flow. Advancing magnetic field leads to a stronger hydromagnetic body force, which reduces fluid and nanoparticle motion. The existence of thermal radiation results in strengthening the flow of molecules besides the nanoparticles. The radiation intensification means a reduction in the absorption coefficient. This reveals the significant role thermal radiation plays on the surface heat transfer, whenever the occurrence of convection heat transfer coefficient is lower.

2. Temperature Profiles

Fig. 6 presents the impacts of thermal radiation with, as well as without, electric field over the thermal profile. Higher values of radiation parameter cause an enhancement of temperature field and thicker thermal layer thickness. This is because the mean absorption coefficient decays with higher values of thermal radiation, which is responsible for the intensification of the thermal field. Hence temperature distribution increases. Presence of the electric field when the thermal radiation is absent reduces the temperature, leading to a thinner thermal-layer thickness to the smallest level of energy. Applying an electric field offers better enhancement of heat transfer due to the stretching sheet surface.

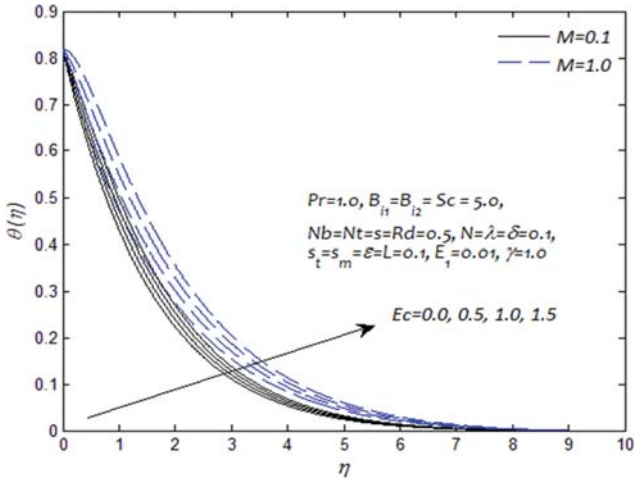

Fig. 7. Strength of Ec on the temperature distribution θ(η).

Intensification in parameter magnetic field M and Eckert number Ec yields higher temperature and thickness of thermal layer as in Fig. 7. A drag-kind of force known as Lorentz strength is created through the magnetic force over electrically-conducting liquid. The nanofluid flows naturally over the surface and experiences an electromagnetic retarding force. Trailing natural convection flow (λ>0) of an electrically conducting nanofluid with the applied magnetic field, the two body forces (buoyancy force and a Lorentz force) interact with each other and, in turn, influence the transport processes of heat and mass. These take a critical role in numerous engineering processes, such as materials manufactured via extrusion practices, and heat treated materials flowing among a feed roll and wind up roll over the surface retain these features. The viscous dissipation connects the relationship between the kinetic energy to the enthalpy difference with respect to the temperature. Higher value of Eckert number implies the cooling of the plate means loss of heat from the plate to the nanofluid. It shows that the interchange over the kinetic energy toward subjective energy as the result

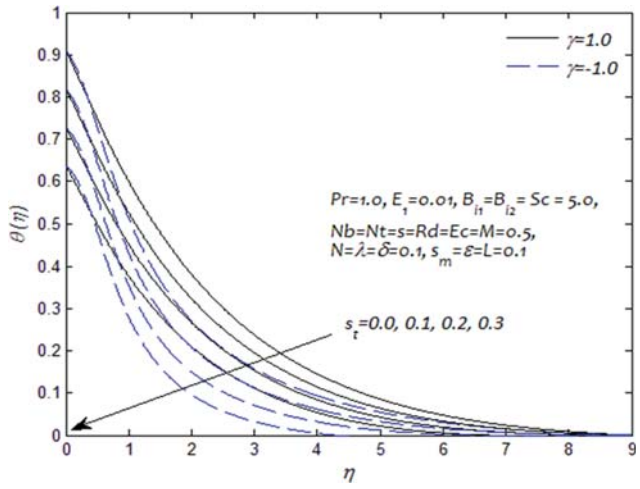

Fig. 8. Strength of s_t on the temperature distribution $\theta(\eta)$.

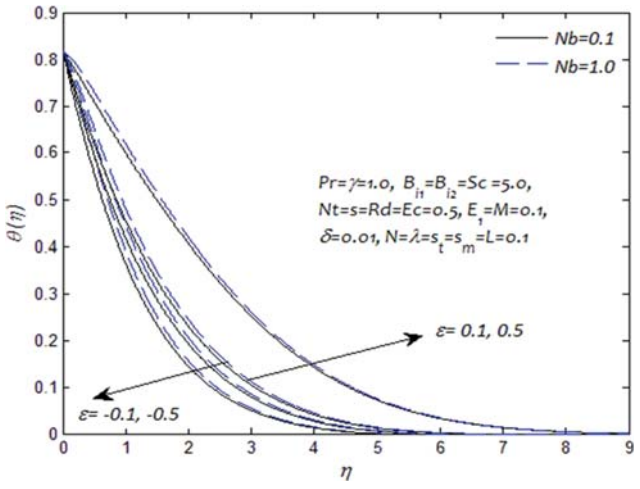

Fig. 10. Strength of ε on the temperature distribution $\theta(\eta)$.

of the work done with the viscous fluid stresses. Dissipation warrants the conversion of the mechanical energy within the downward-flowing fluid to thermal and acoustical energy. Most engineering devices are configured in streambeds to moderate the kinetic energy of flowing fluids, reducing their erosive potential on the fluid surfaces. Consequently, advance dissipative heat produces an increase in the nanofluid temperature.

Fig. 8 illustrates the variation in temperature profile with the stimulus of thermal stratification parameter s_t, destructive chemical reaction parameter ($\gamma>0$) and generative chemical reaction parameter ($\gamma<0$). It was established that temperature distribution considerably declines as the thermal stratification parameter intensifies. The surface temperature drops with an augmentation in thermal stratification. The occurrence in reservoirs can be minimized through vertical mixing of oxygen to the point that bottom fluid becomes anoxic by the action of biological procedures. It reduces more with generative chemical reaction and enhances with destructive chemical reaction near the stretching sheet. This relationship mostly occurs when heat is transferred from a hotter region to a colder region in fluids arising as a result of temperature variation.

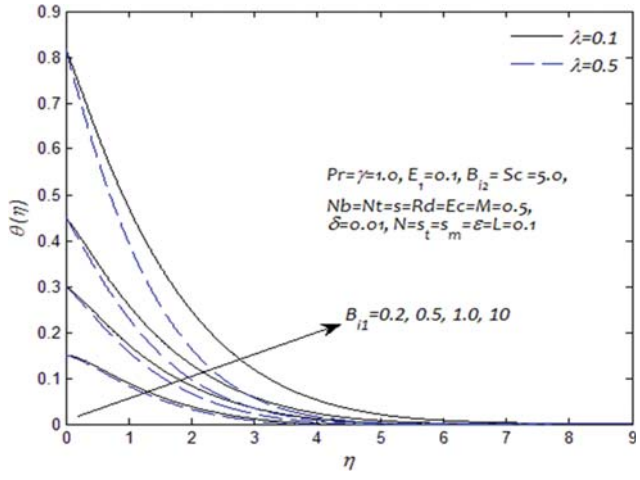

Fig. 9. Strength of B_{i1} on the temperature distribution $\theta(\eta)$.

Fig. 9 shows the behavior of thermal Biot number B_{i1} and mixed convection parameter λ over the thermal field. It signifies an enhancement in the temperature as well as the layer thickness due to thermal Biot number. Essentially, Joule heating forms as a result of flow of electric current conducting nanomaterial-particles beside the molecules. During the collision among the flowing nanoparticles and the molecules some of the kinetic energy is released to heat, leading to intensification of the temperature of the system. Increase in the thermal convective parameter strengthens heat transfer coefficient in addition to thermal layer thickness. The reverse effect was noticed with accumulative mixed convection. At the heated stretching surface locale ($\lambda>0$), the convection current decreases the nanofluid temperature.

The impact of heat generation ($\varepsilon>0$) and absorption ($\varepsilon<0$) with Brownian motion Nb on the temperature profile is depicted in Fig. 10. It is determined that thermal field and layer thickness are strengthened when heat generation intensifies, while reverse effects are noticed during heat absorption. Influence of heat generation accounts for the energy manifestation. Heat generation is significant during removal of nuclear fuel debris, separating fluids in packed-bed reactors, storage of foodstuffs, and underground dumping of radioactive waste solid. In the heat generation mechanism, a great quantity of heat is generated, which leads to an enhancement of temperature profile. Brownian motion raises the thermal field with augmentation in both situations. The behavior shows that they contain the random movement of microscopic nanoparticles suspended in a fluid at the molecular and nanoscale level as this is the process prevailing in the thermal behavior of nanoparticles in nanofluid.

3. Concentration Profiles

Fig 11 demonstrates the effect of Schmidt number Sc and Brownian motion parameter Nb on the concentration profile. Schmidt number takes in the Brownian diffusion coefficient, which decreases with higher values. Hence concentration together with the accompanying thickness-layer decays for intensification. Similar behavior occurred with Brownian motion parameter. The random motion of microscopic, nanoparticles in the fluid at the nanoscale level adds to decay in the concentration. The reason is that the random behavior of the liquid molecules versus particles continues for augmenta-

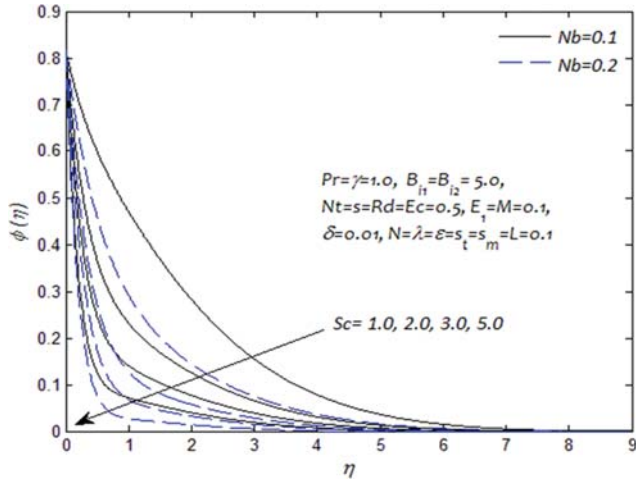

Fig. 11. Strength of Sc on the concentration distribution $\phi(\eta)$.

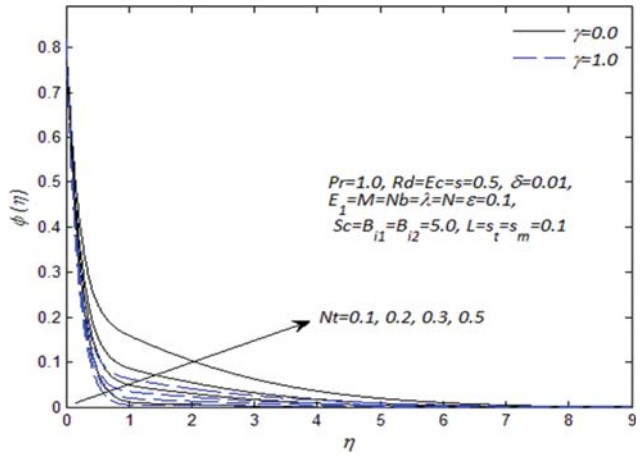

Fig. 12. Strength of Nt on the concentration distribution $\phi(\eta)$.

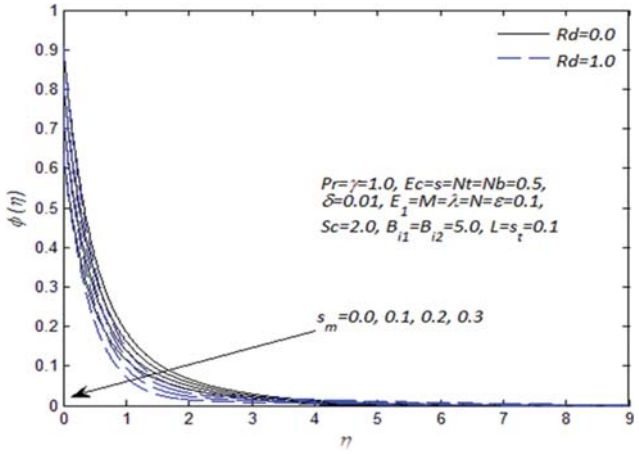

Fig. 13. Strength of s_m on the concentration distribution $\phi(\eta)$.

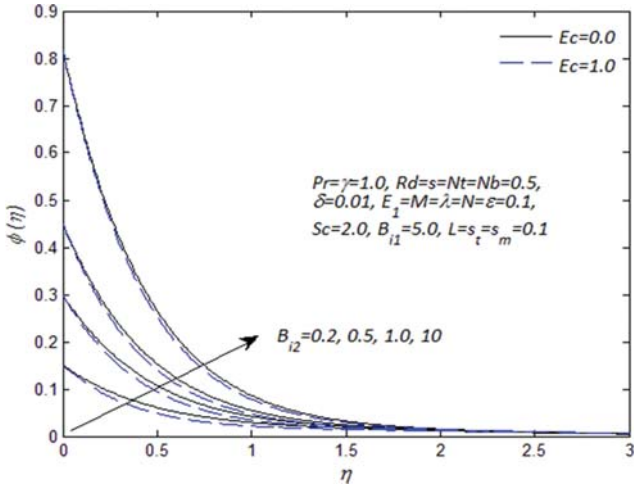

Fig. 14. Strength of B_{i2} on the concentration distribution $\phi(\eta)$.

tion with Brownian flow, resulting in a reduction in the distribution.

In Fig. 12, the flow behavior of thermophoresis parameter Nt and chemical reaction parameter γ are shown with respect to the concentration profile. Higher value of thermophoresis parameter strengthens the thermophoretic force, and this leads to the flow of nanoparticles in the region connected with tendency to minimal thermal energy resulting in intensification. These are attributed to the flow of the nanoparticles' energies from the region of the hot surface to the vicinity of the cold surface. Strong force is witnessed with suspension of nanoparticles as a result of the temperature gradient. The chemical reaction reduces the concentration and layer thickness for an increase in values. This is because in the heterogeneous-chemical-reaction, nanoparticles and fluid-molecules reactants are in different phases.

Fig. 13 portrays the behavior of mass (concentration) stratification parameter s_m and thermal radiation parameter Rd on the concentration profile. It shows that the volumetric fraction sandwiched between the surface and reference nanoparticles decays when mass stratification increases. Thus, the concentration distribution drops, with increase in the flow fields as a result of concentration differences. However, the concentration distribution decreases with the existence of thermal radiation parameter. The coefficient of the mean absorption drops upon intensification, and that accounts for decrease in concentration distribution. This fact yields a decayed trend of the fluid concentration.

Fig. 14 illustrates the power connecting with mass convective Biot number B_{i2} beside Eckert number Ec over the nanoparticle concentration distribution. A great multitude of mass convective Biot number associated with the mass transfer at the surface results in the strengthening of the concentration field. The involvement of mass transfer coefficient intensifies for higher values, which leads to thicker solutal layer thickness. Also, the existence of Eckert number reduces the fluid concentration. The Eckert number measures the loss of energy through flow configuration. It is the relationship between enthalpy difference and the kinetic energy of liquid particles. Because the Eckert number heightens the fluid particles which collide more repeatedly with one another, and hence they tend to release more heat, which leads to decelerating concentration.

4. Skin Friction, Nusselt and Sherwood Numbers

Figs. 15 and 16 portray the differences in the skin friction coef-

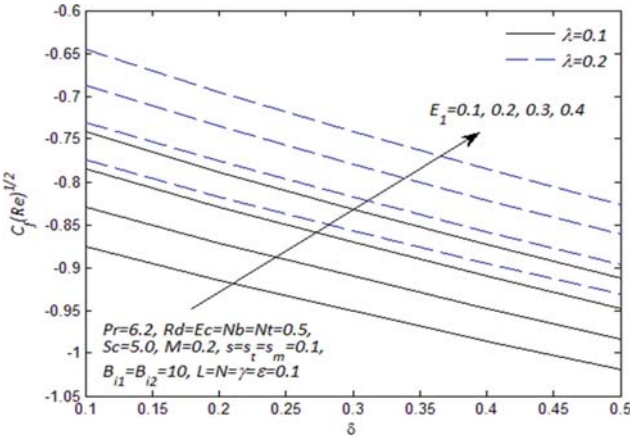

Fig. 15. Influence of E_1 and δ on the skin friction profile.

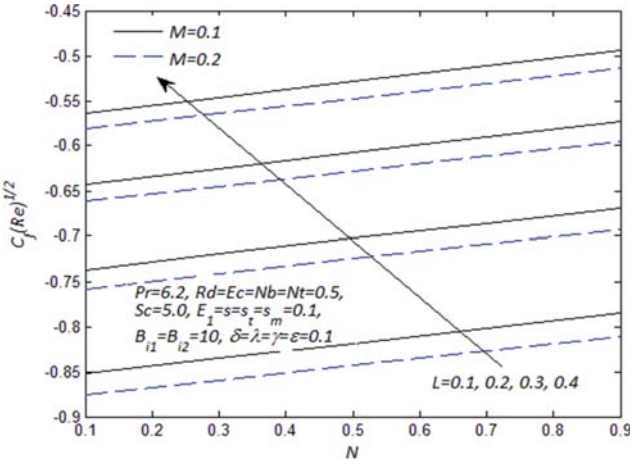

Fig. 16. Effect of L and M on the skin friction profile.

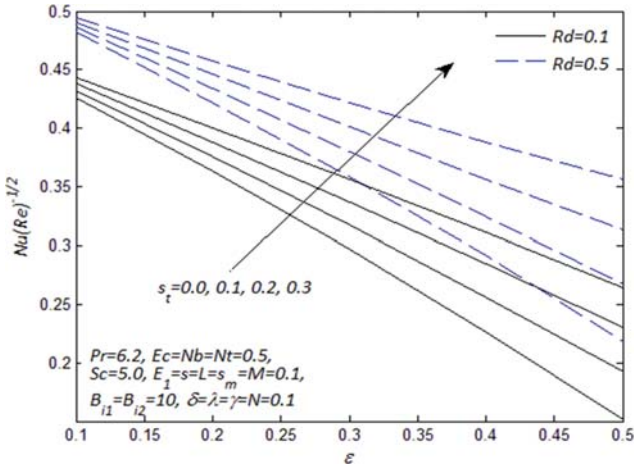

Fig. 17. Influence of s_t and ε on the Nusselt number profile.

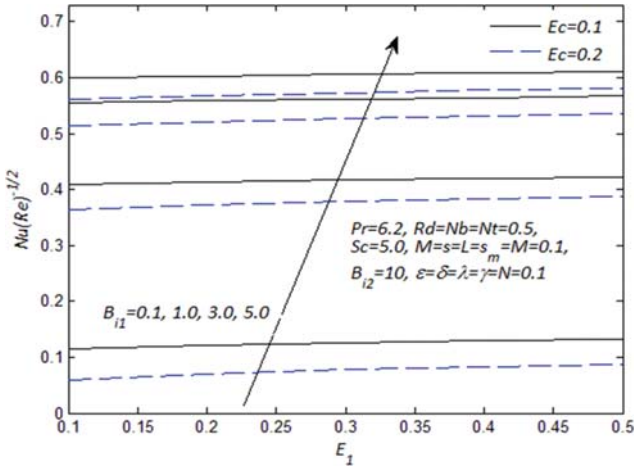

Fig. 18. Influence of B_{i1} and E_1 on the Nusselt number profile.

ficient involving unsteadiness parameter δ, electric field E_1, mixed convection parameter λ, the ratio of concentration to thermal buoyancy forces N, velocity slip parameter L and magnetic field M. The profile decreases with increase in the electric field, but the unsteadiness parameter increases conversely with the mixed convection parameter. This is attributed to the fact that supplementation in δ depreciates the flow field and larger λ gives rise to more buoyancy force. An increase in the values of E_1 reciprocates strongly on the flow of fluid molecules and nanoparticles in the boundary layer. In the vicinity of the stretching medium, reversed behavior occurs with the unsteadiness parameter. As a result, the thinner boundary-layer subsequently lessens the skin friction distribution. The profile drops with upsurge velocity slip parameter L and the ratio of concentration to thermal buoyancy forces N, but rises with magnetic field M. The main physical implication of the results is that both momentum and hydrodynamic layers are reduced, thinned with strong magnetic fields. It is attributed to increases in values of N, and is closely associated with the fluid motion along the stretching surface with nanofluids. The decline in the nanofluid velocity is due to the thermal force applied on the surface, which reduces the flow field. Increase in the ratio of concentration to thermal buoyancy forces as a consequence of the velocity slip decreases the coefficient of the skin friction near the stretching sheet. Consequently, the boundary-layer-thickness declines to justify the skin friction decay. The magnetic field displays the opposite role noticed with the skin friction coefficient profile.

Figs. 17 and 18 show the variation of heat generation ε, thermal stratification s_t, thermal radiation Rd, electric field E_1, heat convective number B_{i1} and Eckert number Ec on the Nusselt number. The profiles rise for increases in thermal radiation parameter and thermal stratification parameter but decrease with heat generation. The temperature between surface and reference temperature drops when s_t advances. Small mean absorption coefficient results in higher radiation parameter, and as a result temperature distribution grows. Consequently, increases in thermal radiation plus thermal stratification cause the motion of nanofluid to concentrate over the layer of the boundary, causing thicker boundary-layers including heightening the Nusselt-number. On the other hand, the existence of viscous dissipation decays the profile, whereas the reverse occurs with the heat convective number B_{i1} beside electric field E_1. The heat convective Biot number has a high dependency relation to the heat transfer at the surface, so larger profile is attributed to higher values of B_{i1}. An increase in the electric field and

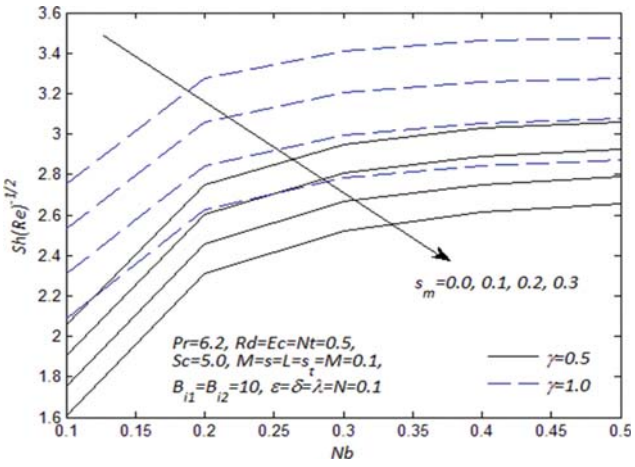

Fig. 19. Influence of s_m and Nb on the Sherwood number profile.

heat convective number increases the rate of heat transfer on the surface sheet and the boundary layer thickness. The Eckert number demonstrates opposite flow behavior accordingly, leading to a reduction of the profile. Physically, as a result of frictional heating, extra kinetic energy is stored in the fluid particles. So, the higher values in temperature difference are reduced at the surface of the sheet.

Fig. 19 establishes the combined consequences of mass stratification parameter s_m, Brownian motion parameter Nb and chemical reaction γ on the Sherwood number profile. Both Nb and γ intensify the mass transfer. Nevertheless, their impacts on wall mass flux are less noticeable from the figure. Higher values of s_m depress the Sherwood number. It is expected that volumetric fraction of nanoparticles between surface and reference concentration drops when solutal stratification is heightened.

The effect of thermophoresis parameter Nt and Schmidt number Sc on wall mass flux with the impact of mass convective Biot number B_{i2} is given by Fig. 20. The mass convective Biot number has extraordinary reliance on mass transfer coefficients. That is, greater mass transfer coefficients lead to heightened concentration. It can be noticed that Sherwood number curves rise for larger values of mass convective Biot number and Schmidt number. Smaller values of mass convective Biot number along with an increase in thermophoresis parameter leads to decay in the wall mass flux.

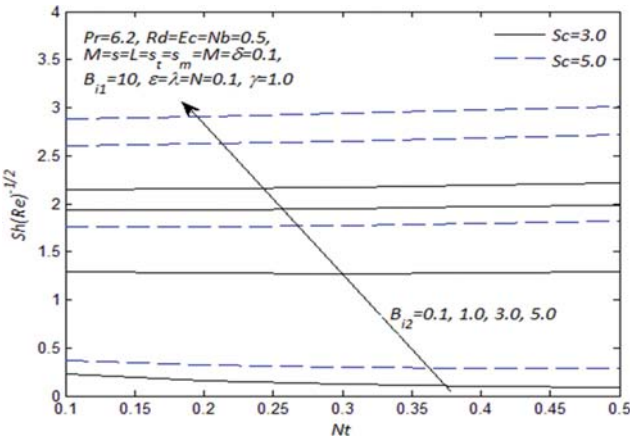

Fig. 20. Influence of B_{i2} and Nt on the Sherwood number profile.

CONCLUDING REMARK

The current study explores the impacts of electric field on unsteady doubly stratified MHD mixed convection slip flow of nanofluid against vertical stretching sheet with the existence of convective heat including mass conditions. In the heat conduction, the accounts of thermal radiation, viscous dissipation, and Ohmic heating with heat generation/absorption were examined. In concentration field, the impact of chemical reaction was considered. The main findings of the study are given below:

1. The convective heat and mass Biot numbers contribute to the enhancement of the temperature and concentration fields as well as thicker layers.

2. Thermal and mass stratification parameters decrease the temperature and concentration fields with an increase in their values.

3. Heat conduction is strengthened by the magnetic field, heat generation, Eckert number, and thermal radiation parameter, but decreases with heat absorption and electric field.

4. Concentration field enhances with lower values of chemical reaction, Brownian motion, and Schmidt number.

5. A higher velocity slip parameter of electric field intensifies the skin friction coefficient, whereas reverse effects occur with mixed convection parameter, unsteadiness parameter and magnetic field for higher values.

6. Increasing the values of thermal stratification, thermal Biot number and radiation parameters increases the Nusselt number, whereas Sherwood number gets strengthened with the chemical reaction parameter, Brownian motion parameter, and Schmidt number.

ACKNOWLEDGEMENTS

The authors would like to acknowledge Ministry of Higher Education and Research Management Centre, UTM for the financial support through HIR grant vote No. Q.J130000.2409.04G43 and COE grant vote No. Q.J130000.2409.03G96 for this research. Also, Yahaya Shagaiya Daniel thankfully acknowledges financial support from TETFUND through Kaduna State University, Nigeria.

NOMENCLATURE

a, b : stretching constants [s^{-1}]
B_0 : strength of magnetic field [$kgs^{-2}A^{-1}$]
B : applied magnetic field [$kgs^{-2}A^{-1}$]
B_{i1}, B_{i2} : heat and mass convective Biot number
c_f : skin friction coefficient [Nm^{-2}]
c_p : specific heat at constant pressure [$JKg^{-1}K$]
D_B : brownian diffusion coefficient [m^2s^{-1}]
D_T : thermophoresis diffusion coefficient [m^2s^{-1}]
E_0 : electric field factor
F_1 : electrical field
E : applied electric field

Ec : Eckert number
f′ : stream function variable
g : acceleration due to gravity [ms^{-2}]
Gr : Grashof number
$\bar{J}$: Joule current
k_1 : rate of chemical reaction
k : thermal conductivity [$Wm^{-1}K^{-1}$]
L : velocity slip constant
M : magnetic field
Nb : Brownian motion parameter
Nt : thermophoresis parameter
Nu : Local Nusselt number
P : pressure [Nm^{-2}]
Pr : Prandtl number
q_r : radiative heat flux [Wm^{-2}]
q_m : wall mass flux
q_w : wall heat flux
Rd : radiation parameter
Re : Local Reynolds number
s_m : concentration stratification constant
s_t : thermal stratification constant
Sc : Schmidt number
t : time [s]
T : temperature [K]
T_0 : reference temperature [K]
T_f : fluid heated temperature [K]
T_∞ : ambient temperature [K]
(u, v) : velocity components onward (x, y) [ms^{-1}]
u_w : stretching velocity [ms^{-1}]
v_w : wall mass transfer

Greek Symbols

β : volumetric coefficient of thermal expansion [K^{-1}]
σ^* : Stefan-Boltzmann constant [$Wm^{-2}K^{-4}$]
ε : heat generation/absorption
σ : fluid electrical conductivity [$s^3A^2kg^{-1}m^{-3}$]
δ : Unsteadiness parameter
η : dimensionless similarity variable
μ : dynamic viscosity of the fluid [Nsm^{-2}]
υ : Kinematic viscosity [m^2s^{-1}]
ρ : density [kgm^{-3}]
ρ_p : particle density [kgm^{-3}]
$(\rho)_f$: density of the fluid [kgm^{-3}]
$(\rho)_c$: heat capacity with respect to the liquid [$Jm^{-3}K^{-1}$]
$(\rho c)_p$: heat capacity with respect to nanoparticle [$Jm^{-3}K^{-1}$]
ψ : stream function
φ : concentration of the fluid [kgm^{-3}]
φ_0 : reference concentration [kgm^{-3}]
φ_f : fluid heated concentration [kgm^{-3}]
φ_∞ : nanoparticle volume fraction at large values [kgm^{-3}]
θ : dimensionless temperature [K]
ϕ : dimensionless concentration [kgm^{-3}]
τ : heat transfer capacity with respect to the liquid equivalent to Heat capacity with respect to the nanofluid
τ_w : surface shear stress [$kgm^{-1}s^{-2}$]
λ mixed convective parameter
γ : chemical reaction constant

Superscript

, : differentiation with respect to η

Subscripts

∞ : quantities at the free stream
m : mass
w : quantities at the wall/surface [ms^{-1}]
0 : reference condition

REFERENCES

1. H. M. Elshehabey and S. E. Ahmed, *Int. J. Heat Mass Trans.*, **88**, 181 (2015).
2. I. Fersadou, H. Kahalerras and M. El Ganaoui, *Comp. Fluids*, **121**, 164 (2015).
3. O. Makinde and I. Animasaun, *Int. J. Therm. Sci.*, **109**, 159 (2016).
4. Y. S. Daniel, Z. A. Aziz, Z. Ismail and F. Salah, *Alex. Eng. J.*, **57**, 2187 (2017).
5. Y. S. Daniel, Z. A. Aziz, Z. Ismail and F. Salah, *Theor. Appl. Mech. Lett.*, **7**(4), 235 (2017).
6. S. U. Choi and J. A. Eastman, Argonne National Lab., IL (United States) (1995).
7. S. Aman, I. Khan, Z. Ismail and M. Z. Salleh, *Neur. Comp. Appl.*, **30**(3), 789 (2018).
8. X. Xiao, T. U. Kang, H. Nam, S. H. Bhang, S. Y. Lee, J. P. Ahn and T. Yu, *Korean J. Chem. Eng.*, **35**(12), 2379 (2018).
9. J. Buongiorno, *J. Heat Transfer*, **128**(3), 240 (2006).
10. M. Rahman, I. Pop and M. Saghir, *Int. J. Heat Mass Trans.*, **129**, 198 (2019).
11. M. Azam, A. Shakoor, H. Rasool and M. Khan, *Int. J. Heat Mass Trans.*, **131**, 495 (2019).
12. M. Irfan, W. Khan, M. Khan and M. M. Gulzar, *J. Phys. Chem. Solids*, **125**, 141 (2019).
13. M. Sheikholeslami, *Comp. Meth. Appl. Mech. Eng.*, **344**, 306 (2019).
14. Y. Bao, T. Wen, A. C. S. Samia, A. Khandhar and K. M. Krishnan, *J. Mater. Sci.*, **51**(1), 513 (2016).
15. S. Mei, C. Qi, T. Luo, X. Zhai and Y. Yan, *Int. J. Heat Mass Trans.*, **128**, 24 (2019).
16. M. I. Khan, T. Hayat, M. I. Khan, M. Waqas and A. Alsaedi, *J. Phys. Chem. Solids*, **125**, 153 (2019).
17. Y. W. Oh, Y. S. Choi, M. Y. Ha and J. K. Min, *Int. J. Heat Mass Trans.*, **132**, 565 (2019).
18. M. D. Garmroodi, A. Ahmadpour and F. Talati, *Int. J. Mech. Sci.*, **150**, 247 (2019).
19. F. Selimefendigil and H. F. Öztop, *Int. J. Mech. Sci.*, **152**, 185 (2019).
20. Y. S. Daniel and S. K. Daniel, *Alex. Eng. J.*, **54**(3), 705 (2015).
21. M. Rashid, M. I. Khan, T. Hayat, M. I. Khan and A. Alsaedi, *J. Mol. Liq.*, **276**, 441 (2019).
22. M. Waqas, T. Hayat, S. Shehzad and A. Alsaedi, *Phys. B: Cond. Matt.*, **529**, 33 (2018).
23. T. Hayat, A. Nassem, M. I. Khan, M. Farooq and A. Al-Saedi, *Phys. Chem. Liq.*, **56**(2), 189 (2018).
24. Y. S. Daniel, A. A. Zainal, Z. Ismail and F. Salah, *Matematika*, **34**(2), 393 (2018).

25. V. Nagendramma, A. Leelarathnam, C. Raju, S. Shehzad and T. Hussain, *Resu. Phys.*, **9**, 23 (2018).
26. Y. S. Daniel, Z. A. Aziz, Z. Ismail and F. Salah, *Aust. J. Mech. Eng.*, 1 (2018).
27. M. Ramzan, M. Bilal and J. D. Chung, *Int. J. Mech. Sci.*, **131**, 317 (2017).
28. Y. S. Daniel, Z. A. Aziz, Z. Ismail and F. Salah, *Chin. J. Phys.*, **55**(3), 630 (2017).
29. Y. S. Daniel, Z. A. Aziz, Z. Ismail and F. Salah, *J. Comp. Design Eng.*, **5**(2), 232 (2017).
30. Y. S. Daniel, Z. A. Aziz, Z. Ismail and F. Salah, *J. Appl. Res. Technol.*, **15**(5), 464 (2017).
31. M. Ramzan, M. Bilal, J. D. Chung and A. Mann, *Neur. Comp. Appl.*, **30**(9), 2739 (2018).
32. Y. S. Daniel, Z. A. Aziz, Z. Ismail and F. Salah, *Aust. J. Mech. Eng.*, 213 (2018).
33. S. Shehzad, T. Hayat and A. Alsaedi, *Bull. Poli. Acad. Sci. Technol. Sci.*, **63**(2), 465 (2015).
34. T. Hayat, M. Waqas, S. Shehzad and A. Alsaedi, *J. Mol. Liq.*, **215**, 704 (2016).
35. T. Hayat, A. Shafiq and A. Alsaedi, *Plos One*, **9**(1), e83153 (2014).
36. N. Freidoonimehr, M. M. Rashidi and S. Mahmud, *Int. J. Ther. Sci.*, **87**, 136 (2015).
37. M. Nayak, N. S. Akbar, V. Pandey, Z. H. Khan and D. Tripathi, *Powder Technol.*, **315**, 205 (2017).
38. Y. S. Daniel, Z. A. Aziz, Z. Ismail and F. Salah, *Eng. Lett.*, **26**(1), 107 (2018).
39. M. Farooq, Q. ul ain Anzar, T. Hayat, M. I. Khan and A. Anjum, *Resu. Phys.*, **7**, 3078 (2017).
40. T. Hayat, M. Waqas, M. I. Khan and A. Alsaedi, *J. Mol. Liq.*, **225**, 302 (2017).
41. T. Cebeci and P. Bradshaw, Springer Science & Business Media (2012).
42. F. Mabood, W. Khan and A. M. Ismail, *J. Magn. Magn. Mater.*, **374**, 569 (2015).
43. W. Ibrahim and B. Shankar, *Comp. Fluids*, **75**, 1 (2013).
44. D. Pal and H. Mondal, *Comm. Nonl. Scie. and Num. Simu.*, **15**(5), 1197 (2010).
45. T. Hayat, M. Imtiaz and A. Alsaedi, *Int. J. Heat Mass Trans.*, **92**, 100 (2016).
46. T. Hayat, M. Waqas, M. I. Khan and A. Alsaedi, *Int. J. Heat Mass Trans.*, **102**, 1123 (2016).
47. P. Besthapu, R. U. Haq, S. Bandari and Q. M. Al-Mdallal, *J. Taiw. Inst. Chem. Eng.*, **71**, 307 (2017).
48. M. Khan and M. Azam, *J. Mol. Liq.*, **225**, 554 (2017).